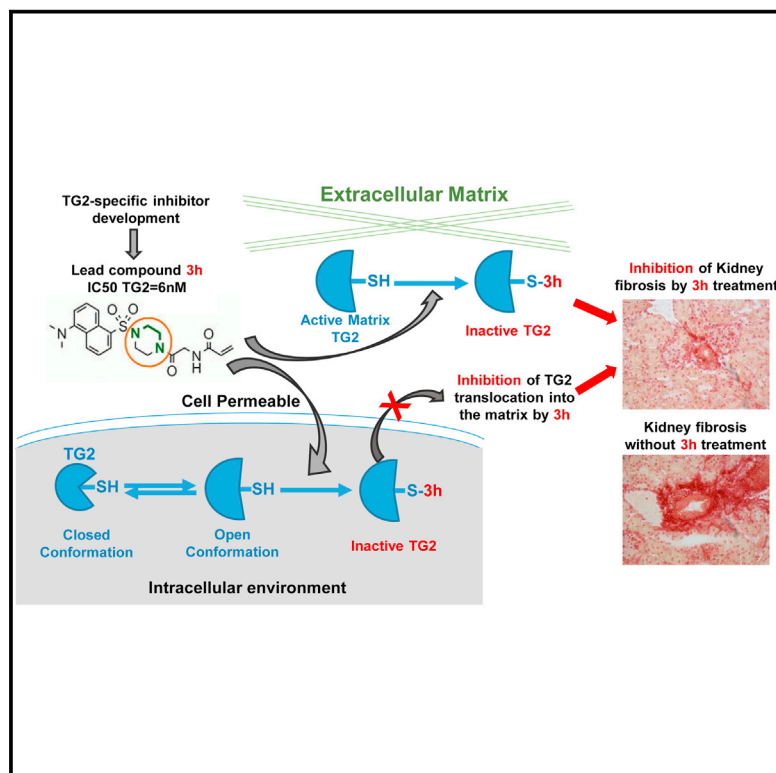


Chemistry & Biology

Development of Potent and Selective Tissue Transglutaminase Inhibitors: Their Effect on TG2 Function and Application in Pathological Conditions

Graphical Abstract



Authors

Eduard Badarau, Zhuo Wang, Dan L. Rathbone, ..., Said El Alaoui, Milda Barkeviciute, Martin Griffin

Correspondence

m.griffin@aston.ac.uk

In Brief

Badarau et al. design and develop high-potency TG2-specific irreversible inhibitors that show reactivity with the intracellular active form of TG2, leading to inhibition of its translocation into the extracellular matrix. The compounds are effective in inhibiting in vitro angiogenesis and hypertensive nephrosclerosis in animal models.

Highlights

- Irreversible tissue transglutaminase (TG2) inhibitors of high selectivity and potency
- Target the Ca²⁺ activated form of TG2 in the intra- and/or extracellular space
- Reactive with intracellular TG2 and block its translocation into the matrix
- Effective in blocking hypertensive nephrosclerosis in animal models

Development of Potent and Selective Tissue Transglutaminase Inhibitors: Their Effect on TG2 Function and Application in Pathological Conditions

Eduard Badarau,^{1,4,5} Zhuo Wang,^{1,4} Dan L. Rathbone,¹ Andrea Costanzi,¹ Thomas Thibault,¹ Colin E. Murdoch,² Said El Alaoui,³ Milda Barkeviciute,² and Martin Griffin^{1,*}

¹School of Life and Health Sciences, Aston University, Aston Triangle, Birmingham B4 7ET, UK

²Aston Medical Research Institute, Aston Medical School, Aston University, Aston Triangle, Birmingham B4 7ET, UK

³Covalab France, 11 avenue Albert Einstein, 69100 Villeurbanne, France

⁴Co-first author

⁵Present address: European Institute of Chemistry and Biology, 2 Rue Robert Escarpit, 33607 Pessac, France

*Correspondence: m.griffin@aston.ac.uk

<http://dx.doi.org/10.1016/j.chembiol.2015.08.013>

SUMMARY

Potent-selective peptidomimetic inhibitors of tissue transglutaminase (TG2) were developed through a combination of protein-ligand docking and molecular dynamic techniques. Derivatives of these inhibitors were made with the aim of specific TG2 targeting to the intra- and extracellular space. A cell-permeable fluorescently labeled derivative enabled detection of in situ cellular TG2 activity in human umbilical cord endothelial cells and TG2-transduced NIH3T3 cells, which could be enhanced by treatment of cells with ionomycin. Reaction of TG2 with this fluorescent inhibitor in NIH3T3 cells resulted in loss of binding of TG2 to cell surface syndecan-4 and inhibition of translocation of the enzyme into the extracellular matrix, with a parallel reduction in fibronectin deposition. In human umbilical cord endothelial cells, this same fluorescent inhibitor also demonstrated a reduction in fibronectin deposition, cell motility, and cord formation in Matrigel. Use of the same inhibitor in a mouse model of hypertensive nephrosclerosis showed over a 40% reduction in collagen deposition.

INTRODUCTION

Transglutaminases (TGs) belong to a family of protein crosslinking enzymes that catalyze an acyl transfer reaction between the γ -carboxamide group of peptide-bound glutamine and the ϵ -amino group of peptide-bound lysine (or a suitable primary amine) resulting in formation of a $\epsilon(\gamma$ -glutamyl)lysine isopeptide bond (Griffin et al., 2002). In mammals, eight catalytically active TGs, each Ca^{2+} -dependent, are found in this family, of which tissue transglutaminase (TG2) is probably the most ubiquitous in human tissues. The current challenges in studying the role of TG2 are to (1) develop inhibitors that target TG2 and not other members of the TG family (specificity); (2) investigate independently the intracellular and extracellular roles of the enzyme (cell permeability); (3) characterize the effect of

specifically inhibiting TG2 crosslinking activity in physiological/pathological conditions. TG2 is involved in a host of human diseases such as celiac disease, cancer, fibrosis, multiple sclerosis, and neurodegeneration (Wang and Griffin, 2012). As a consequence, TG2 has become a potential therapeutic target for the treatment of these pathological conditions (Badarau et al., 2013a). Moreover, since TG2 is found both in the intra- and extracellular space, both targeted specificity for TG2 itself and specific targeting to a particular subcellular space are needed.

We recently described inhibitors aimed at targeting only the extracellular space (Badarau et al., 2013b; Griffin et al., 2008). These molecules incorporate two key polar groups in their structure in order to assure their high hydrophilic character: a carboxylate moiety and a charged warhead represented either by a dimethylsulfonium (Griffin et al., 2008) or by an imidazolium function (Badarau et al., 2013b). Despite their activities in the low micromolar range, these derivatives have great potential because of their high aqueous solubility and their excellent cellular toxicity profile. In fact, since their intracellular access is restrained, these inhibitors show very little toxicity in cells up to 750 μM over 72 hr (Wang and Griffin, 2013). They have also shown considerable success in proof-of-concept studies in animal models of kidney fibrosis over 120 days without any signs of toxicity but with significant improvements in kidney function (Huang et al., 2009; Johnson et al., 2007). However, the major drawback with these extracellular acting TG inhibitors is potency and specificity. Therefore, the first objective of our work was to design potent, highly specific TG2 inhibitors that could be used for targeting the intra- and/or extracellular space, were not toxic in cellular systems, and had the potential to be used in preclinical studies.

In the design of this new family of inhibitors, we were also very much aware that, once deposited into the extracellular matrix (ECM), TG2 is tightly associated with its potential substrates and is not easily accessible; and that the secretion and translocation of TG2 onto the cell surface and into the extracellular matrix ECM, which is independent of the conventional ER/Golgi pathway, requires the binding of TG2 to the cell surface heparan sulfate proteoglycan syndecan-4. Importantly, the binding of TG2 to this proteoglycan is highly favored by its compact closed conformation (Wang et al., 2012; Lortat-Jacob et al., 2012). Hence, a further objective in this work was to assess whether

suitably labeled irreversible TG2 specific inhibitors that can permeate the cell can also bind TG2 inside the cell thus both inhibiting enzyme activity and locking it into its open confirmation. This is particularly important when considering TG2 as a therapeutic target since TG2 in its open confirmation is likely to be blocked in its translocation to the cell surface and into the ECM because it is unable to bind effectively to cell surface heparan sulfates (Wang et al., 2012). Moreover, if it does manage to reach the ECM, e.g. from cell lysis, it reaches it in an inactive form. Such inhibitors are likely to have a broad spectrum of application in TG2-mediated human pathologic conditions in which TG2 is acting either inside or outside the cell.

RESULTS

In developing the TG2 inhibitors, the work was divided into two interlinked processes: *in silico* molecular modeling to first design and then synthesize the inhibitors and then a series of studies on their characterization. The latter included enzyme potency, specificity, cell permeability, solubility, and *in vitro* ADME (absorption, distribution, metabolism, excretion) characterization followed by an assessment of their potential application in biological systems using cell-based and *in vivo* preclinical models.

Generation of New Peptidomimetic TG2 Inhibitors

Molecular modeling was used to yield insights into the probable binding pattern of our previous peptidic water-soluble derivatives. The modeling approach was based on the Michaelis-Menten complexes generated by docking of these compounds with the open conformation of TG2 (PDB: 2Q3Z). These were then subsequently “relaxed” by molecular dynamics conducted in explicit water at 300 K (see [Supplemental Experimental Procedures](#)).

The trajectories generated provided a rich source of information that helped in the development of the new TG2 inhibitors. One of the successfully exploited pathways relied on the observation that, during the dynamics trajectory, the water-soluble ligands tend to adopt a specific conformation in the central amino acid region. In fact, the dihedral N1-C2-C3-N4 emphasized in [Figure 1A](#) stabilized around 0° with a limited variation of ±20°. This key observation was the starting point for the design of a new series of inhibitors.

In order to mimic the observed conformation for the central N1-C2-C3-N4 region, we next introduced a piperazine scaffold, as indicated in [Figure 1B](#). The same three-atom linker was preserved between N4 and the carbonyl (vicinal to the warhead), however, in order to facilitate the subsequent chemical modifications, a new nitrogen atom was introduced. One of the first structures synthesized to validate this “restrained conformation” hypothesis exhibited the same activity range as the initial water-soluble substrates (**1a**, [Figure 1B](#)). The irreversibility of the inhibitors was first confirmed by prior incubation of the compounds with recombinant purified human TG2 and then subsequent dilution prior to assay of the incubated enzyme as previously described (Griffin et al., 2008). An indication of the hydrophilic character of this derivative was observed experimentally during the isolation step by freeze-drying the aqueous layer after separation from the organic layer. In addition, an indication of its cellular toxicity profile was undertaken in human umbilical

cord endothelial cells (HUVECs). As very little cellular toxicity was observed after 72 hr at concentrations up to 100 μM ([Figure S1](#)), this new molecule (**1a**) represented the starting point for subsequent modifications. To rule out the effect of any potential TG2 and FXIII present in the serum from the cell culture medium, which could eliminate the effect of the compounds in the toxicity assay, the HUVECs were cultured in serum-free endothelial cell medium in the presence of compounds **3h**, **1h**, and **3e** up to 72 hr, with no significant toxicity detected at the concentrations used ([Figure S2](#)).

Optimization of Inhibitor Potency

The first step of our modification strategy focused on the central amino acid region of the newly designed ligands. In order to evaluate the effect of steric hindrance that could be generated by additional substituents in this position, derivatives bearing new core amino acids were synthesized ([Figure 1C](#), Schemes 1 and 2). As summarized in [Table 1A](#), the activity was lost when using bulky substituents arising from phenylalanine (**1l**, **1k**), the same but more moderate trend being observed for small substituents (**1i**, **1j**). It should also be mentioned that the chirality of the stereogenic carbon atom seemed important, the analog in the L-Ala series (**1i**) being favored over its D isomer (**1j**).

Our attention next focused on the electrophilic warhead region. Different groups were tested in order to evaluate their influence on the binding process. As a possible means of targeting the extracellular space by limiting cell permeability, highly polar warheads were attached to the newly designed skeleton. As shown in [Table 1B](#), the dialkylsulfonium moieties retained a good inhibition range (**1a**, **1q**), while the imidazolium warhead induced a complete loss of activity (**1s**). It should be noted that, in our initial water-soluble peptidic inhibitors, the same imidazolium warhead maintained a good TG2 inhibition range (Badarau et al., 2013b), suggesting the binding patterns of the two classes of inhibitors are very different.

Our next approach was to design inhibitors containing lipophilic warheads, which were more likely to be cell permeable and could be used to target the intracellular space. As the catalytic CYS residue was revealed by the different available crystal structures of TG2 to be hosted in a narrow tunnel (PDB: 2Q3Z, Pinkas et al., 2007; PDB: 1KV3, Liu et al., 2002; PDB: 3LY6, Han et al., 2010), our choice was focused on terminal Michael acceptors such as acrylamides and vinylsulfonamides. Such warheads possess an additional carbon atom in the electrophilic region of the ligand, and it is likely that this will induce a different conformation of the warhead around the catalytic CYS residue compared with the sulfonium-based inhibitors. [Table 1B](#) shows that both of these new warheads preserved a good inhibition range (**2a**, **3a**), the vinylsulfonamide having a more favorable effect on binding.

Other modifications were performed in the carbamate region ([Table 1C](#)). As this moiety was predicted by modeling to bind in the hydrophobic pocket of the binding site (as revealed by the crystal structure of the open-form conformation; Pinkas et al., 2007), different-size aromatic carbamates were tested in the first instance. In this case, the corresponding bromide precursors originally developed for inhibiting the serine proteases (Schoellmann and Shaw, 1963), and which have high reactivity with the enzymatic nucleophile, were also biologically evaluated.

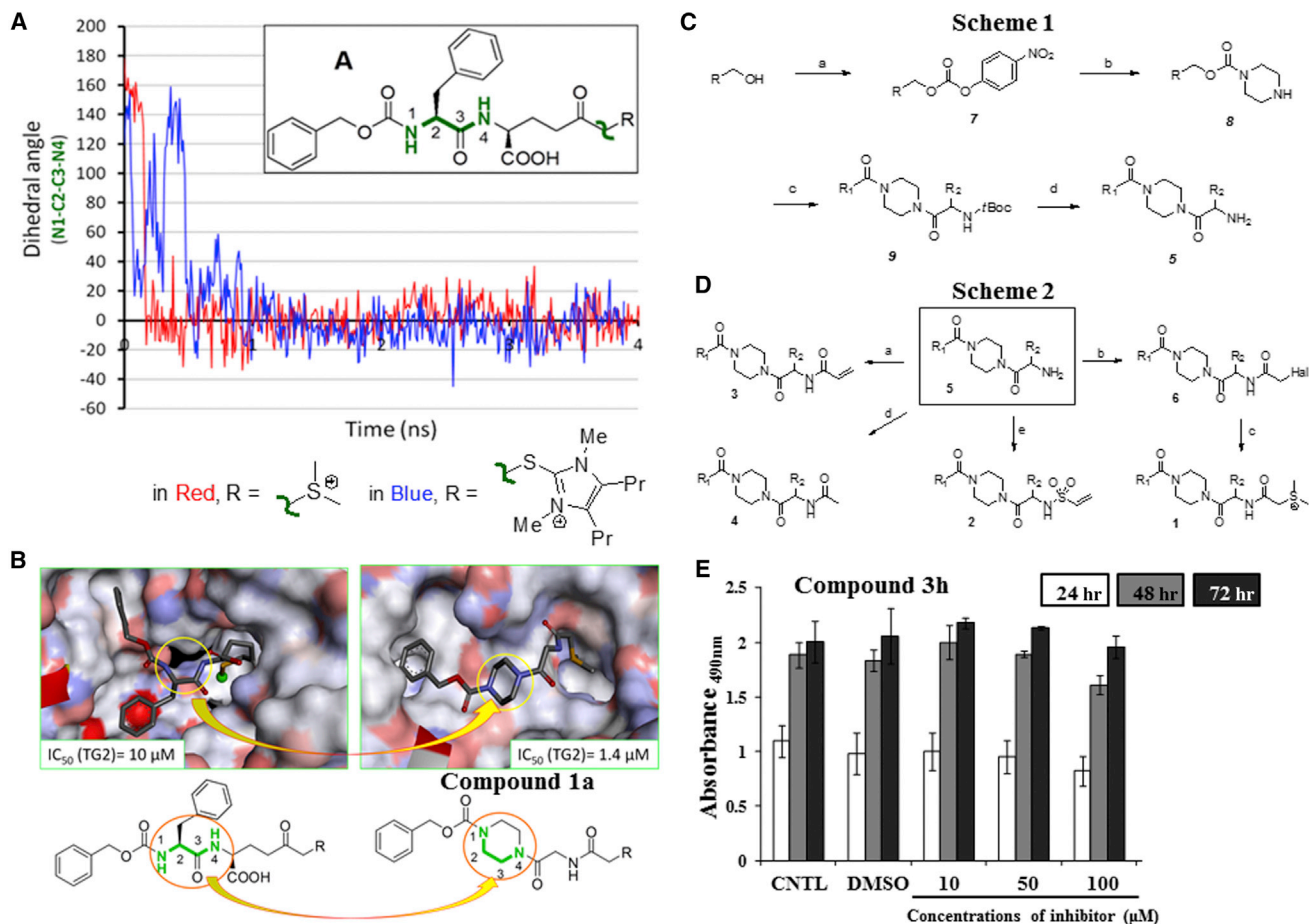


Figure 1. Design and Synthesis of Lead TG2 Inhibitor Precursor

(A) Examples of dihedral angles defined by N1-C2-C3-N4 recorded during the molecular dynamics trajectory.

(B) Design of new peptidomimetic derivatives starting from the water-soluble inhibitors, R = SMe_2 .

(C) Scheme 1 for the synthesis of the amine precursors. (a) *p*-NO₂-phenylchloroformate, N-methylmorpholine (NMM)/dichloromethane (DCM), 0°C, 2 hr; (b) piperazine, triethylamine (TEA)/dimethylformamide, 0°C to room temperature, 12 hr; (c) *tert*-butyloxycarbonyl (*t*-Boc)-Glu-OH, 1-ethyl-3-(3-dimethylaminopropyl) carbodiimide, HOBt, NMM/DCM, room temperature, 12 hr; (d) trifluoroacetic acid/DCM, room temperature, 24 hr. Commercially available alcohols were activated as *p*-nitrophenyl carbonates **7** and subsequently reacted with piperazine at room temperature in order to give the desired mono-carbamates **8**. A peptidic coupling step with *t*-Boc-protected amino acids, followed by the acidic deprotection of the amines conducted to the key intermediates **5**.

(D) Scheme 2 for the synthesis of the final derivatives. (a) Acryloyl chloride, TEA/acetonitrile, 0°C to room temperature, 3 hr; (b) bromoacetyl bromide or chloroacetyl chloride, TEA/DCM, -78°C to room temperature, 12 hr; (c) dimethylsulfide/MeOH, room temperature, 24 hr; (d) acetyl bromide, TEA/DCM, -78°C, 2 hr; (e) 2-chloroethylsulfonyl chloride, TEA/DCM, -60°C-0°C, 4 hr. Starting from the previously obtained amines **5**, various acylation agents were used in order to obtain the final derivatives **1-4** as summarized in Scheme 2. In the case of polar dimethylsulfonium warhead, an additional nucleophilic substitution step was conducted on the halomethylamide precursor **6**.

(E) Toxicity profile of the fluorescent derivative **3h** on HUVEC lines, after 24 hr (white), 48 hr (gray), and 72 hr (black) as described in the [Experimental Procedures](#). CNTL, control.

If for the dimethylsulfonium and acrylamide warheads the inhibition varies in the lower micromolar range, for the corresponding halomethylketones the potency was increased to the lower nanomolar range. However, their high cellular toxicity profile for the halide precursors, particularly the more reactive bromides, confirmed their limited pharmacological use.

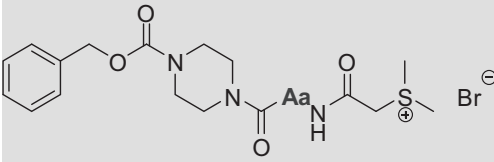
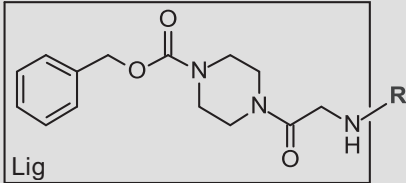
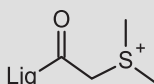
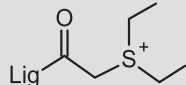
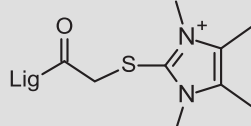
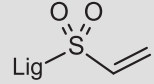
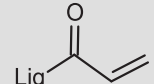
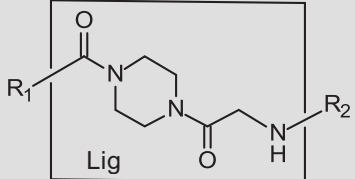
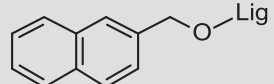
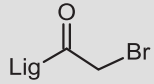
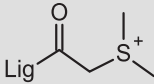
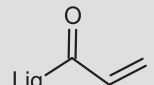
A new set of inhibitors was prepared following the same hypothesis of targeting the hydrophobic pocket of the active site. An adamantyl moiety was chosen as the reference substituent and its distance from the piperazine ring was systematically varied in order to find an optimum for the interaction with the enzyme. The corresponding *tert*-butyl carbamate was also

synthesized. The best median inhibitory concentration (IC₅₀) in the “lipophilic” series was obtained for the acrylamide warhead (**3e**), while in the “hydrophilic” series, the *tert*-butyl carbamate (**1m**) outperformed its analogs ([Table 1C](#)).

Design and Characterization of a Fluorescent Probe and Further Characterization of Lead Compounds

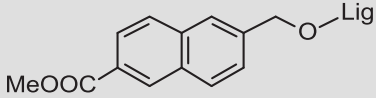
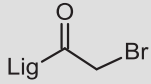
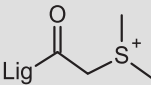
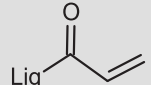
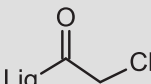
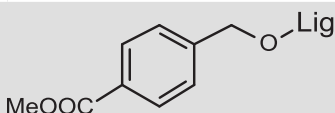
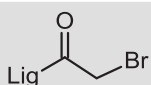
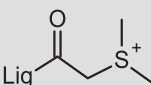
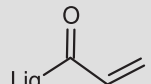
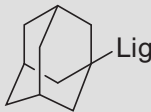
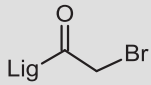
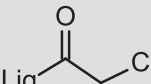
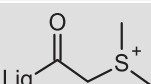
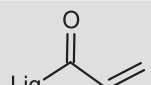
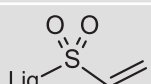
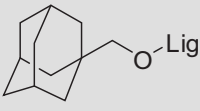
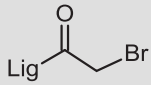
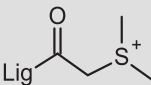
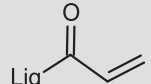
A dansyl fluorescent tag was attached to the central piperazine scaffold to fully exploit the biological potential of this new class of TG2-specific inhibitors, with the view to being able to pin point and visualize the presence of the inhibitors, most importantly the presence of the active enzyme located at a cellular level. Analogs

Table 1. TG2 Inhibition Data on Varying the Central Amino Acid, the Warhead on the Initial Hit, and the Substituents in the Carbamate Region

(A) Central Amino Acid:			(B) Warhead on the Initial Hit:		
					
Compound	Aa	IC ₅₀ (μM ± SD)	Compound	R	IC ₅₀ (μM ± SD)
1a	Gly	1.4 ± 0.5	1a		1.4 ± 0.5
1j	D-Ala	6.8 ± 2.0	1q		1.85 ± 0
1i	L-Ala	0.7 ± 0.3	1s		100
1l	D-Phe	>100	2a		1.725 ± 0.11
1k	L-Phe	>100	3a		5.925 ± 0.11
(C) Substituents in the Carbamate Region:					
					
Compound	R ₁	R ₂	IC ₅₀ (μM ± SD)		
6c			0.029 ± 0.019		
1c			1.07 ± 0.1		
3c			0.44 ± 0.057		

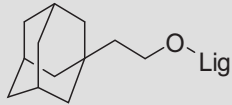
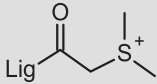
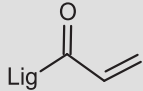
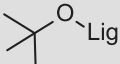
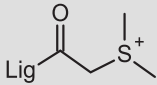
(Continued on next page)

Table 1. Continued

6d			0.015 ± 0.007
1d			1.5 ± 0.4
3d			2.1 ± 0
6n			0.00665 ± 0.00021
6b			0.0021 ± 0.0004
1b			3.3 ± 0.3
3b			6.3 ± 2.9
6e			0.0039 ± 0.0004
6o			0.00875 ± 0.00035
1e			0.889 ± 0.2
3e			0.125 ± 0.066
2e			0.875 ± 0.035
6f			0.00629 ± 0.0005
1f			0.775 ± 0.035
3f			1.625 ± 0.035

(Continued on next page)

Table 1. Continued

1g			3.15 ± 0.92
3g			0.9 ± 0.14
1m			0.273 ± 0.11

IC₅₀ values accompanied by the SD were averaged from at least three independent experiments; they were otherwise obtained in a single experiment.

in both water-soluble and lipophilic series were obtained and evaluated for their activity on a battery of TGs (Table 2A). Compound **3h** had an excellent IC₅₀ of ~6 nM for TG2, as well as a good toxicity profile when tested up to 100 μM (Figure 1E), and showed selectivity for TG2 when assayed against TG1, TG3, TG6, and Factor XIIIa (FXIIIa). A comparable TG selectivity profile was also shown for **1h** with an IC₅₀ value of 380 nM, again with a good toxicity profile (Figure S1).

Measurement of the K_i and K_{inact} of **3h** and **1h** using the glutamate dehydrogenase coupled assay indicated high potency, particularly **3h**, with a K_{inact} of 0.387 min⁻¹, a K_i of 1.31 μM, and a K_{inact}/K_i of 297,692 min⁻¹ M⁻¹. This was comparable with the other high-potency non-dansylated inhibitor **3e** (IC₅₀ 125 nM), which had a calculated K_{inact} of 0.275 min⁻¹, a K_i of 1.63 μM, and a K_{inact}/K_i of 171,875 min⁻¹ M⁻¹. The other fluorescent inhibitor, **1h**, in line with its lower IC₅₀ (380 nM), had a K_i of 57 μM, a K_{inact} of 0.337 min⁻¹, and a K_{inact}/K_i of 5,830 min⁻¹ M⁻¹. Given the potential application of **3h** and **1h** in TG2 conformational studies, it was important to demonstrate that their reactivity was Ca²⁺ dependent. For this, recombinant human TG2 was incubated for 30 min at 4°C with either Ca²⁺ (1 mM) or GTP (1 mM), and then for a further 30 min in the presence of compound **3h** (10 nM) or **1h** (1 μM). Spin columns were then used to remove excess inhibitor. Evaluation of TG2 activity after removal of the excess inhibitor indicated that only the enzyme incubated with GTP was active (Figure 2A), thus confirming the requirement of Ca²⁺ for the inhibitors **3h** and **1h** to access the transamidating active site.

To rule out potential off-target effects of the inhibitors, inhibition of the cysteine proteases Caspase 3 and 7 was undertaken. HUVECs were induced into apoptosis and the caspase activity measured in situ in the presence and absence of **3h** and **1h**. No inhibition of Caspase 3 or 7 was shown (Figure 2B). The same results were obtained for the inhibitors **1e** and **3e**, which carry the dimethylsulfonium and the acrylamide warheads, respectively.

Other potent compounds were also tested for their specificity toward TG2 compared with other TG family members. Biotinylated TG-specific glutamine-containing peptides specific for TG family members, including TG1, FXIIIa, TG3, and TG6, were used in these assays (CovTests; Perez Alea et al., 2009). Comparable IC₅₀ values of these inhibitors for TG2 were detected in both the CovTest and the biotin-cadaverine incorpora-

tion assay. All derivatives from this series proved selective over the TG1, TG3, and FXIIIa TGs with selectivity shown against TG6 for compounds **1e**, **1f**, and **3f** although less selectivity was shown for TG6 with compound **3e** (Table 2B). A moderate TG1 inhibition trend was observed for the halomethylamides. In the case of TG2, however, the inhibition activities are in the lower nanomolar range (>100-fold selectivity ratio). To rule out any non-specific reaction of the inhibitors with TG1, TG3, and FXIIIa, the dansylated probes **3h** and **1h** were incubated with these three isoforms in the presence of Ca²⁺ and with EDTA, enzymes were then separated by denaturing SDS gel electrophoresis and western blotted for the detection of the dansyl group, which showed negligible reactivity of the TG isoforms with either inhibitor (Figure S3).

Further Characterization of the TG2 Inhibitors

Toxicity Studies

The toxicity profile of some of these new potent inhibitors was evaluated in HUVECs using the XTT-based assay as described previously (Wang and Griffin, 2013). The toxicity varied between 25 and 100 μM (Table S1 and Figure S1). As expected, in relation to their high reactivity, the halomethylketones (**6n**, **6o**) were the most toxic compounds. The more hydrophilic inhibitors bearing the dimethylsulfonium warhead were well tolerated by the same cell lines with toxicity thresholds of <100 μM. Encouraging results were also obtained for the compounds designed to be more lipophilic, especially **3e**, which has an inhibition activity for TG2 in the nanomolar range (IC₅₀ = 0.125 ± 0.066 μM). Different toxicity profiles were observed between the acrylamide- and vinylsulfonamide-based derivatives (**3e** vs **2e**), which might be explained in part by their different chemical reactivities.

Confirmation of Covalent Interaction and Targeting the Active Site Cys277 by **1h** and **3h**

The fluorescent inhibitor probes allowed us to demonstrate that these compounds were targeting the active site Cys277 in their covalent reactivity. Pure recombinant wild-type (wt) TG2 and its active site mutant Cys277Ser were incubated with the compound **1h** in the presence of Ca²⁺ for 3 hr. As a positive control, the wt enzyme was incubated with the competitive amine substrate monodansylcadaverine (MDC), which becomes enzymatically incorporated into available γ-glutamyl residues on neighboring TG2 molecules.

Table 2. Inhibition profiles (IC₅₀) for different TGs for both fluorescent derivatives and other selected potent TG2 inhibitors

(A)							
Compound	FXIIIa (μM)	TG1 (μM)	TG3 (μM)	TG6 (μM)	TG2 (μM)	PSA (Å ²)	R
3h	>100	25	20	5	0.0061 ± 0.00042	90	Lig—
1h	>100	>100	>100	>10	0.38 ± 0.057	112	Lig—
3e	37	2.2	11	2	0.125 ± 0.066	70	Lig—
(B) Compound							
	IC ₅₀						
	TG1 (μM)	TG3 (μM)	TG6 (μM)	FXIIIa (μM)			
1a	>100	>100	NT	>100			
1c	>100	>100	NT	>100			
3c	>100	>100	NT	>100			
6d	5	65	NT	>100			
1d	>100	>100	NT	>100			
3d	>100	>100	NT	>100			
1b	>100	>100	NT	>100			
6e	1	70	NT	>100			
1e	>100	>100	>10	>100			
6g	3	50	NT	>100			
1f	>100	>100	>10	>100			
3f	>100	>100	>10	>100			
3g	>100	>100	NT	>100			
1m	>100	>100	NT	>100			

For (A) in the case of TG2, the inhibition data (IC₅₀) accompanied by standard deviation (SD) were averaged from at least three independent experiments using the biotin cadaverine incorporation assay. For TG1, TG3, TG6 and Factor XIIIa the commercial TG-CovTest assay was used (Hitomi et al., 2009; Fukui et al., 2013) with data obtained from one experiment. The polar surface area (PSA) values were calculated as described in the Supplemental Experimental Procedures (B) Shows mean IC₅₀ values obtained in a single experiment undertaken in duplicate using the commercial TG-CovTest assay. NT = not tested.

Following incubation, TG2 was separated on denaturing SDS-PAGE and western blotted using an anti-dansyl antibody (Figure 2C). Bands were seen in the positive control containing the MDC and in the wt enzyme where the active site Cys277 is intact, indicating covalent interaction of the inhibitor with TG2. In the Cys277Ser mutant, no incorporation of MDC was detected in a band that was indicative for TG2. Presence of the inhibitor was not detected with the Cys277Ser mutant, suggesting that fluorescent inhibitor **1h** is specifically targeting the active site Cys277.

Cellular Permeability

The cellular permeability profile for a subset of compounds was investigated using the irreversible imidazolium-based inhibitor **R283** (Freund et al., 1994), which is cell permeable, and the peptidic inhibitor **R281**, which is cell impermeable, as reference as described previously (Baumgartner et al., 2004). This assay is

based on the ability of compounds to permeate the cell and inhibit intracellular TG2 activity after its activation by the elevation of intracellular Ca²⁺ using ionomycin. As initially designed, the assay confirmed that acrylamide-based inhibitors **3e**, **3f** and the fluorescent probe **3h** penetrate the cell and inhibit intracellular TG2 activity, contrary to the charged compounds **1e** and **1f** (Figure 2D). As a means of validating the permeability assay used in these studies, the cell permeability of compounds **3h**, **3e**, and **1h** was also determined in MDCKII-MDR1 cells. The assay was conducted in the presence of the efflux transporter inhibitor GF120918. Using this assay, the passive permeability (P exact) of compounds **3h**, **1h**, and **3e** was 649, 1.3, and 676 nm/s respectively, confirming that the acrylamide inhibitors **3h** and **3e** are cell permeable. In contrast, the positively charged **1h** is cell impermeable. Measurement of the thermodynamic solubility of these same three compounds in PBS (pH 7.4) over 24 hr was 24 μM for **3h**, 1594.6 μM for **1h**, and 698 μM for **3e**.

co-immunoprecipitation (co-IP) studies. NIH3T3 cells transduced with wt TG2 were used to confirm whether the intracellular reaction of **3h** with TG2 could take place. Figure 2E shows that inhibitor **3h** permeates into NIH3T3 cells and reacts with intracellular TG2, which can be increased further in the presence of the Ca²⁺ ionophore ionomycin (Figure 2E). This is demonstrated by co-IP of the inhibitor/TG2 complex in the cytosolic fraction of cells using an anti-dansyl antibody and TG2 revealed in this complex using an anti-TG2 antibody by western blotting. Importantly, the reactivity of **3h** with intracellular TG2 was reduced by incubating in the presence of the cell-permeable inhibitor **3e** (Figure 2E).

To confirm that the newly developed fluorescent inhibitors **3h** or **1h** only interact with TG2 in its open Ca²⁺ bound conformation and lock the enzyme into this conformation, wt recombinant TG2 pre-treated with Ca²⁺ or GTP was incubated with inhibitor **3h** and then separated by native PAGE. As shown in Figure 2F, **3h** and **1h** in the presence of Ca²⁺ bind to TG2 and hold it in its open conformation, while the binding of GTP, which holds TG2 in its closed conformation, blocks the interaction of **3h** or **1h** with TG2 and gives rise to increased mobility.

HUVECs, which contain high levels of endogenous TG2, were also used to verify our observations in TG2-transduced NIH3T3 cells. Cells were incubated in the absence or presence of the Ca²⁺ ionophore ionomycin (positive control). Mouse endothelial cells isolated from TG2^{-/-} mice were used as the negative control together with HUVECs incubated with **3h** in the presence of the cell-permeable non-dansylated inhibitor **3e**. After fixation of the cells and removal of any excess inhibitor by washing, fluorescence microscopy revealed a faint intracellular dansyl signal in the HUVECs without ionomycin treatment, which was increased with ionomycin and reduced in the presence of inhibitor **3e**. No dansyl signal was detected in the negative control mouse endothelial cells, which are null for TG2 after fixing and washing out any excess inhibitor (Figure 3A). Further confirmation that the dansyl inhibitor is targeting TG2 was obtained by co-IP of the dansyl-labeled proteins in the cell cytosol fractions of cell lysates and the detection of TG2 by western blotting. TG2 was found to be present in the HUVECs with or without ionomycin. The signal was reduced in the cells treated with the inhibitor **3e** and, importantly, as found with immunofluorescent microscopy, totally absent in the TG2^{-/-} mouse endothelial cells (Figure 3B). Hence, in both TG2-transduced NIH3T3 cells and in HUVECs, TG2 appears to be present in the intracellular environment in an open conformation and able to react with inhibitor **3h**, suggesting that the enzyme could be active if suitable substrates are available to it, or, dependent on its environment, is simply alternating between the open and closed conformation.

Effect of **3h** on TG2 Interaction with Syndecan-4 and its Translocation to the Cell Surface and ECM

The interaction between TG2 and syndecan-4 has been reported to be not only essential for the externalization of the enzyme onto the cell surface and deposition into the ECM (Wang et al., 2012) but also for its pathological roles in fibrosis (Scarpellini et al., 2014). Previous work from us and others suggested the importance of TG2 crosslinking activity in pathological conditions such as fibrosis, angiogenesis, and multiple

sclerosis. Therefore, we next studied the effect of inhibitor **3h** on the binding of TG2 to syndecan-4 and its subsequent translocation into the ECM.

It has been reported that TG2 binding to syndecan-4 is favored by the compact conformation (Wang et al., 2012) of the enzyme. It has been shown in Figure 2F that the inhibitor **3h** locks TG2 into its open conformation, which would have a significant impact on the binding of the enzyme to syndecan-4. Therefore, we next studied the effect of **3h** binding to TG2 on the enzyme's binding to cell surface heparan sulfates. Figure 3C shows that in NIH3T3 cells, previously used to show TG2 binding to cell surface syndecan-4, **3h** significantly reduced the interaction between TG2 and cell surface syndecan-4 following co-IP of TG2 with anti-syndecan-4 antibody as previously documented (Wang et al., 2012). Importantly, in these same cells, binding of TG2 to **3h** led to a dramatic reduction in the presence of the enzyme on the cell surface and in the ECM (Figure 3D), which paralleled a dramatic reduction in the deposition of fibronectin (FN) into the ECM (Figure 3D).

Effects of Fluorescent TG2 Inhibitor **3h** on Endothelial Cell Function

In our previous report, using our first generation of peptidic TG inhibitors, we showed that extracellular TG2 could be a potential target in the treatment of VEGF-induced angiogenesis due to its ability to block the deposition of FN, which is one of the important ECM proteins required for matrix-bound VEGF signaling (Wang et al., 2013). Given the ability of compound **3h** to react with both intracellular and extracellular HUVEC TG2, we tested the effects of compound **3h** on different but related endothelial cell functions. Figure 4A shows that inhibitor **3h** reduced the deposition of FN into the ECM by HUVECs, which agrees with its effect in NIH3T3 cells (Figure 3D). One further role of TG2 in endothelial cell angiogenesis is in cell migration during tubule formation (Wang et al., 2013), which is dependent on the cross-linking activity of the enzyme. Figures 4B and 4C demonstrate that compound **3h** inhibited HUVEC migration in the wound-healing assay and in Matrigel cord formation assays.

Potency of Inhibitor **3h** in an In Vivo Model of Hypertensive Nephrosclerosis

As a further means of demonstrating the potential application of these new peptidomimetic inhibitors in human disease where TG2 has been shown to act extracellularly, we next looked at the effects of inhibitor **3h**, which blocks both intracellular and extracellular TG2 activity, on angiotensin II (AngII)-induced hypertensive nephrosclerosis in mice. Before undertaking these studies, we first gained an approximate cell IC₅₀ for **3h** by looking at the inhibition of FN deposition in HUVECs and in mouse endothelial cells, which in both cases gave an approximate IC₅₀ for **3h** of 0.3 μM in human HUVECs and 0.4 μM in mouse endothelial cells (Figure S4).

AngII and **3h** were delivered using a subcutaneously implanted osmotic minipump (Azlet) over 14 days. Mice receiving AngII alone together with inhibitor vehicle showed signs of increased collagen deposition around the arterioles and, in some cases, in the glomeruli and interstitial tubular space. In contrast, animals receiving AngII plus compound **3h** showed significantly reduced (approx. 40%) collagen deposition in all these regions (Figure 5A)

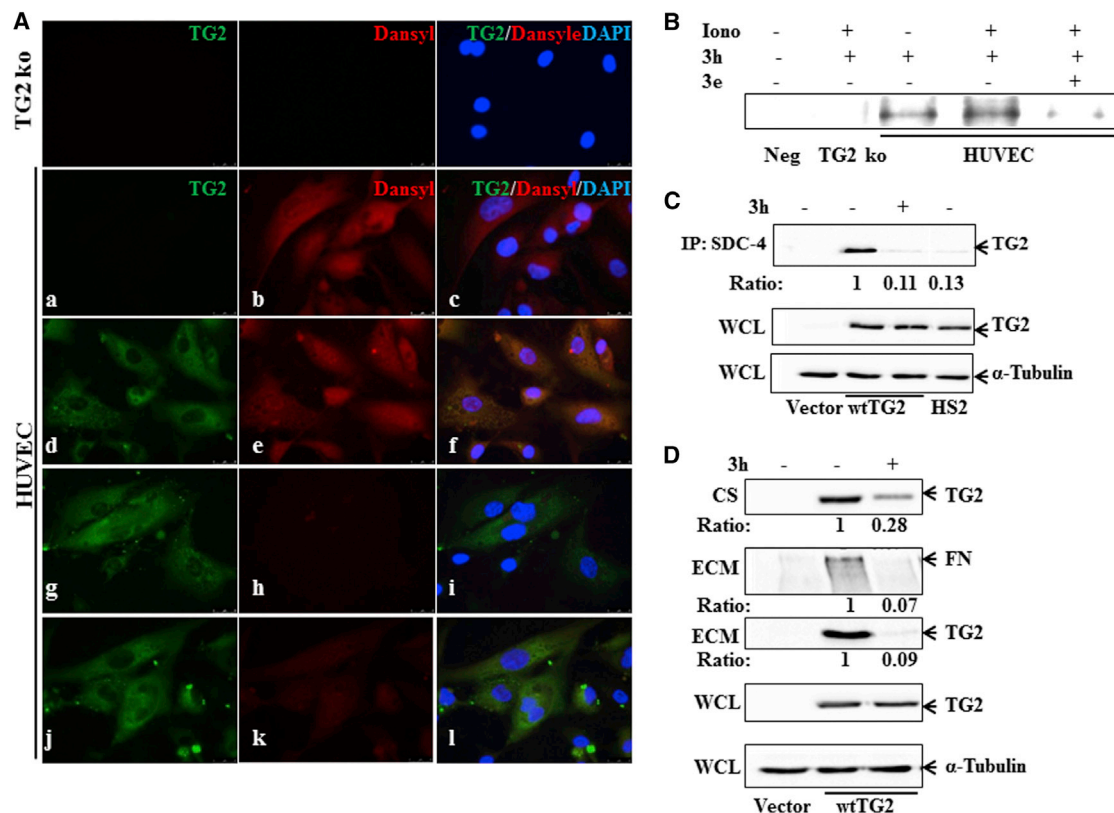


Figure 3. Intracellular Reactivity of Fluorescent Compound 3h with TG2 and its Effect on Enzyme Externalization

(A) Detection of in situ TG2 activity using the dansyl derivative **3h**, HUVECs and TG2^{-/-} mouse endothelial cells (top panel) were treated as described in the [Experimental Procedures](#). The cells were pre-treated with (a–i) or without ionomycin (j–l), in the presence (g, h) or absence (a–f and j–l) of non-dansylated cell-permeable inhibitor **3e**, while TG2 antigen was visualized using anti-TG2 antibody Cub7402 (d–l). DAPI is shown in the top right hand corner of each image. (B) Detection of TG2-dansyl derivative **3h** complex in HUVECs and mouse TG2^{-/-} endothelial cells after co-IP and western blotting. HUVECs were treated as described in (A). Cytosol fractions were collected and co-IP was undertaken using an anti-dansyl antibody as described in the [Experimental Procedures](#). The presence of TG2 was detected via western blotting. Rabbit IgG and TG2 knockout endothelial cells were used as the negative controls. (C) Effect of inhibitor **3h** on the interaction between TG2 and syndecan-4. Swiss3T3 cells transduced with wt TG2 were pre-treated with inhibitor **3h**. Co-IP was performed using anti-syndecan-4 antibody to pull down the immune complex and the presence of TG2 was detected via western blotting. The empty vector transduced cells (vector) or the heparan sulfate binding mutant (HS2) TG2-transduced cells were used as the controls. (D) Effect of **3h** on TG2 externalization and deposition. The presence of TG2 in Swiss3T3 cells from (C) was detected via biotinylation of cell surface (CS) proteins followed by western blotting. The matrix proteins were collected as described in the [Experimental Procedures](#) and the presence of TG2 was measured using anti-TG2 antibody Cub7402 via western blotting. WCL, whole-cell lysate.

with around 45% reduction around the blood vessels (Figure 5B) in the kidneys of inhibitor-treated animals. No obvious signs of toxicity were observed in the animals after inhibitor treatment.

DISCUSSION

In this paper, we report a new series of small-molecule peptidomimetic inhibitors that are selective for TG2 activity. Importantly, we also demonstrate the biological impact of these inhibitors and demonstrate their potential application in both cell and animal models for the targeting of TG2 in diseases such as fibrosis and pathological angiogenesis.

Contrary to the classic family of TG2 inhibitors represented mainly by the peptidic inhibitors, this new series adds a new member to the modest, but continuously increasing, family of non-peptidic TG2 inhibitors. Sporadic examples have been disclosed so far (Duval et al., 2005; Klock et al., 2011; Ozaki

et al., 2010, 2011; Pardin et al., 2008a, 2008b; Prime et al., 2012; Schaertl et al., 2010). Their pharmacological characterization in terms of potency, specificity, binding-site targeting, toxicity, and cellular permeability still remains to be revealed. In addition, a more recent report screening existing TG2 inhibitors based on a weak electrophilic 3-bromo-4,5-dihydroisoxazole (DHI) scaffold showed poor selectivity against TG1 (Klock et al., 2014). Constructed on a piperazine core, this new scaffold presented here has the advantage of an excellent selectivity profile at least against four other members of the TG family that were evaluated during our studies (TG1, TG3, TG6, and FXIIIa). It should be noted, however, that another two groups (Prime et al., 2012; Wityak et al., 2012) have reported piperazine-based derivatives with interesting TG2 activities; however, Prime et al. (2012) reported that their selectivity over the other TGs (especially over FXIIIa) requires further optimization. Wityak et al. (2012) reported that their lead inhibitor had an IC₅₀ for TG2

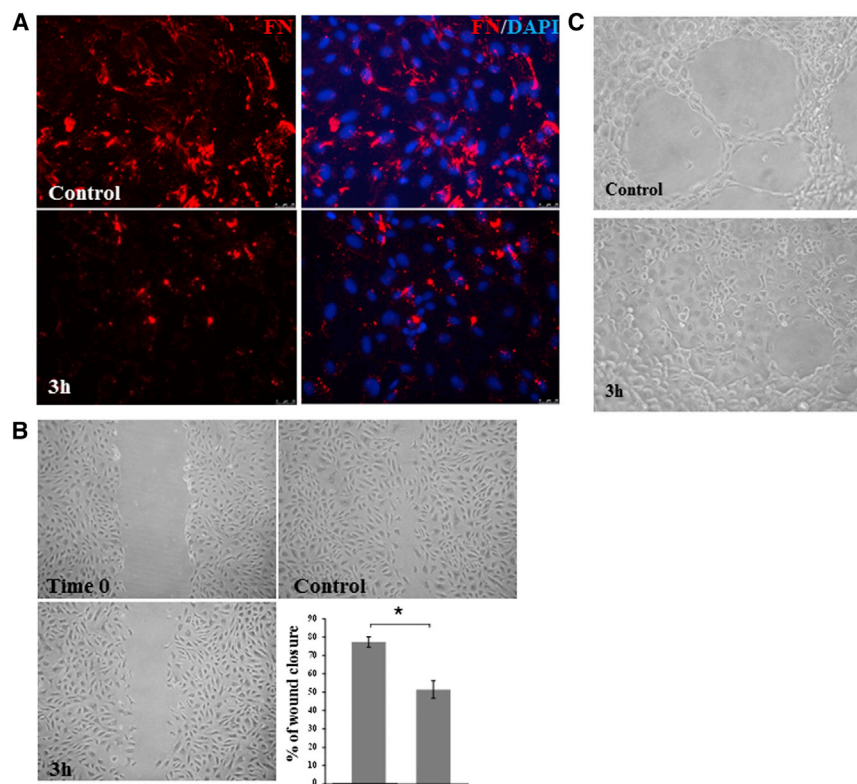


Figure 4. Effect of Compound 3h on Endothelial Cell Migration and Tubule Formation

(A) Representative images showing the effect of **3h** on FN deposition by HUVECs. 7×10^4 HUVECs were seeded into chamber slides in the presence or absence of **3h** treatment for 72 hr. Immunofluorescence staining was performed to detect the extracellular FN as described in the [Experimental Procedures](#). Fluorescence images were captured using an epifluorescence microscope from three separate experiments.

(B) Representative images showing the effect of **3h** on HUVEC migration in the wound-healing assay. HUVECs were seeded into 12-well plates until confluency. Wounds were introduced into the monolayer using 200- μ l tips. The cells were allowed to migrate for 6 hr and the closure of the wounds was analyzed using ImageJ software ($n = 3$). * $p < 0.05$.

(C) Representative images demonstrating the inhibition of HUVEC cord formation on Matrigel by **3h**. 96-well plates were pre-coated with Matrigel and HUVECs were allowed to form cord structures for 6 hr. The images from three separate experiments were taken using a Nikon digital camera.

(Wang and Griffin, 2012; Wang et al., 2013). The development of a highly potent cell-permeable fluorescent inhibitor specific for TG2, allowed us to test for the

of 14 nM with selectivity over TG1, TG3, TG6, and FXIIIa but no cell or animal studies were undertaken on these compounds although in vitro DMPK studies indicated they had low toxicity; the authors indicated that improved ADME profiling was still required for in vivo applications because of their low plasma stability. Importantly, the straightforward synthetic route of the compounds presented in this report gives easy access to various modulations, allowing us to improve the toxicity profile of our inhibitors up to 100 μ M/72 hr, while controlling their cellular access. However, like the compounds reported by Wityak et al. (2012), further improvements on ADME characteristics are still necessary for some of our lead compounds, in particular improvements in microsomal stability and aqueous solubility for **3h**, although solubility may not be such an issue for in vivo potency given that the solubility of **3h** is $>3,000$ times the IC_{50} of **3h**. Moreover, the poor microsomal stability of **3h** is unlikely to be due to the piperazinyl moiety as suggested by Wityak et al. (2012) given that compound **1h**, which is a comparable structure apart from the warhead, is microsomal stable.

Physiologically, TG2 is an enzyme that exists both in the intra- and extracellular environment. Inside the cell, its Ca^{2+} -dependent crosslinking activity is thought to be tightly controlled by the binding of GTP/GDP, which holds the enzyme in a compact closed inactive conformation (Bergamini et al., 2011; Wang and Griffin, 2012). However, TG2 is reported to be involved in a number of human diseases where it acts both intracellularly (e.g. cystic fibrosis, cancer progression, epidermal growth factor receptor recycling) (Bergamini et al., 2011; Zhang et al., 2013) and/or extracellularly, including matrix deposition, tissue fibrosis, VEGF-dependent angiogenesis, and multiple sclerosis

first time whether TG2, when inside the cell, can indeed exist in both its potentially active open conformation as well as its closed/compact conformation. Our data suggest that reactivity of TG2 with the fluorescent inhibitor probe can take place in the low Ca^{2+} intracellular environment of both HUVECs and NIH3T3 cells, which can be further enhanced by using the Ca^{2+} ionophore ionomycin. Given that the reported K_m app for Ca^{2+} for TG2 is around 3 μ M (Hand et al., 1985), this suggests that the conformation of the enzyme may also be regulated by other binding factors in addition to Ca^{2+} , which permits flexibility between the open and compact conformation and which, when in the open conformation, allows the irreversible reaction with the fluorescent TG2 inhibitor probe. Earlier fluorescence resonance energy transfer studies with TG2 have also suggested that, in certain localities of the cell, the enzyme may exist in its open conformation (Pavlyukov et al., 2012). This may explain a number of observations where TG2 has been reported to regulate a several cellular processes either through conformational changes that regulate protein binding (Zhang et al., 2013) or via its transamidating activity (Colak et al., 2011).

As referred to earlier, TG2 can be secreted into the ECM by a non-conventional mechanism, which requires the cell surface binding of heparan sulfates, such as syndecan-4, for its translocation into the ECM. This binding of TG2 to syndecan-4 at the cell surface is favored by the enzyme being in its compact closed conformation, suggesting that the enzyme is secreted in this conformation or that this conformation is assumed once it reaches the cell surface (Wang et al., 2012). Therefore, our next question was to ask if the binding of an irreversible inhibitor inside the cell, which would hold the enzyme in its open

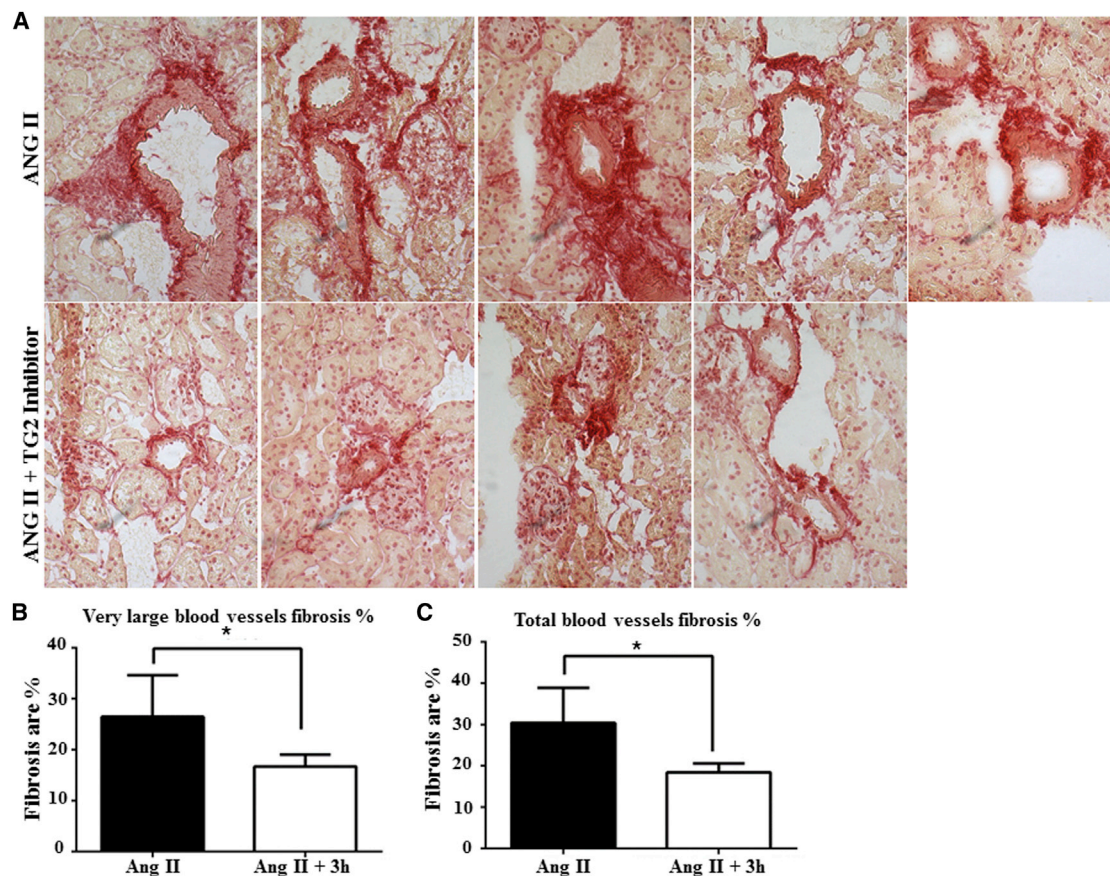


Figure 5. TG2 Inhibition Attenuates Angiotensin II-Induced Renal Fibrosis

Two groups of animals were used. In the first group, five C57BL/6 male mice (14 weeks old) were infused with AngII 1.1 mg/kg/day in 50% DMSO in PBS (pH 7.4) for 2 weeks without TG2 inhibitor via a subcutaneously implanted osmotic pump (Alzet 1002) as previously described (Murdoch et al., 2014). In the second group, compound **3h** was infused in a similar manner at 25 mg/kg/day in 50% DMSO in PBS (pH 7.4) together with AngII over 14 days.

(A) Representative images of kidneys from the inhibitor- (lower panel) and non-inhibitor- (upper panel) treated animals.

(B and C) Averaged data of Sirius red/collagen staining in kidney sections showing staining (B) around arterioles (n = 4) and (C) total collagen staining (n = 5). *p < 0.05.

conformation, would interfere with both its translocation to the cell surface and its deposition into the ECM.

Using NIH3T3 cells, we clearly show that treatment of these cells with the fluorescent permeable inhibitor **3h** reduces the presence of TG2 at the cell surface and nearly completely blocks translocation of the enzyme into the ECM, a finding that is accompanied by the reduced deposition of FN. In HUVECs, where we know TG2 also reacts with our fluorescent probe inside the cell, we also observed a large reduction in the deposition of FN in the presence of this TG2 inhibitor. In relation to biological functions of endothelial cells, this intracellular acting probe is also a potent inhibitor of endothelial cord formation on Matrigel and a potent inhibitor of endothelial motility, which is required for endothelial tube formation (Wang et al., 2013). As a further means of demonstrating the potential application of the new peptidomimetic inhibitors in in vivo studies in a disease state where TG2 acts extracellularly, we next looked at the effects of inhibitor **3h** on AngII-induced hypertensive nephrosclerosis in mice. Mice receiving AngII plus compound **3h** showed significantly reduced (approx. 40%) collagen deposition across all

regions of the kidney with around a 45% reduction in collagen deposition around the kidney arterioles when compared with mice receiving AngII and vehicle.

Hence, our findings demonstrate that our new peptidomimetic TG2 small-molecule inhibitors, which can react with TG2 inside the cell and prevent export of the enzyme as well as block its activity, provide an ideal therapeutic avenue for the treatment of human diseases involving TG2.

SIGNIFICANCE

TG2 has been shown to be essential in a number of human disease states, including fibrosis and angiogenesis. However, other transglutaminase family members sharing a similarity in their structures generate obstacles in generating TG2-specific inhibitors with high potency and low toxicity. Using molecular dynamics techniques, a series of new peptidomimetic inhibitors against TG2 were produced with excellent selectivity when tested against four other members of the transglutaminase family (TG1, TG3, TG6,

and FXIIIa). A highly potent TG2 cell-permeable fluorescent probe ($IC_{50} = 6$ nM; $Kinact/Ki$ of $297,692 \text{ min}^{-1} \text{ M}^{-1}$) was designed and exploited in several biological studies. We demonstrate that the reactivity of the inhibitor can take place with TG2 in the low Ca^{2+} intracellular environment of HUVECs and NIH3T3 cells, which is enhanced by using the Ca^{2+} ionophore ionomycin. Importantly, reaction of TG2 with this fluorescent inhibitor led to a loss of binding of TG2 to cell surface syndecan-4 in NIH3T3 cells and inhibition of TG2 translocation into the ECM, which was paralleled by a reduction in the deposition of matrix FN. Further studies with HUVECs treated with this cell-permeable fluorescent inhibitor revealed a significant reduction in FN deposition, cord formation on Matrigel, and cell motility. As a means of demonstrating the potential application of the new peptidomimetic inhibitors in vivo, where TG2 acts extracellularly (Huang et al., 2009; Johnson et al., 2007), the effects of inhibitor 3h on Angiotensin II (AngII)-induced hypertensive nephrosclerosis in mice was investigated. Mice receiving AngII plus compound 3h showed significantly reduced (approx. 40%) collagen deposition across all regions of the kidney with around 45% reduction around blood vessels. Hence, this new series of TG2-specific cell-permeable peptidomimetic inhibitors may be highly effective in targeting human diseases involving extracellular TG2 via their ability to block both protein crosslinking activity and enzyme export.

EXPERIMENTAL PROCEDURES

Synthetic and Analytical Methodology

The newly synthesized derivatives were characterized by IR spectroscopy, proton and carbon-13 nuclear magnetic resonance spectroscopy (^1H - and ^{13}C -NMR), melting points, high resolution mass spectrometry, and had properties consistent with the proposed structures (see Supplemental Experimental Procedures).

Biological Methodology

General experimental procedures were performed as described previously (Wang et al., 2012, 2013, Wang and Griffin, 2012) and experimental information is detailed in the Supplemental Experimental Procedures.

Reagents and Antibodies

The general reagents were purchased from Sigma-Aldrich (UK), unless stated otherwise.

Chemical Synthesis of the Inhibitors

The synthesis of the inhibitors is described in the Supplemental Experimental Procedures.

Cell Culture

HUVECs (Lonza) (Wang et al., 2013) and NIH3T3 cells (Wang et al., 2012) were cultured as described previously (Supplemental Experimental Procedures).

TG2 Activity Assays

For measurement of TG2 activity, the incorporation of biotinylated cadaverine into immobilized *N,N*-dimethylcasein was used as described previously (Wang et al., 2012).

For determination of the activity of TG1, TG3, TG6, and FXIIIa, commercial microassays were used (TG-CovTest; Covalab) (Hitomi et al., 2009), according to the manufacturer's instructions. For comparable purposes, a number of TG2 assays were also undertaken using this assay. Briefly, TG-specific biotinylated peptides, including pepF11KA (FXIII pre-activated with thrombin), pepK5 (TG1), pepT26 (TG2), pepE51 (TG3), or pepY25 (TG6) (Hitomi et al., 2009; Fukui et al., 2013) were incubated with suitable TG family members in

the presence of polyamine substrates immobilized onto 96-well microplates. The incorporated biotinylated peptides were measured using horseradish peroxidase-conjugated streptavidin and then measured using *o*-phenylenediamine dihydrochloride substrates. The absorbance was measured at 490 nm using a microplate reader.

Glutamate Dehydrogenase Coupled Assay Used for Kinact/Ki Calculations

TG2 inhibitors were assayed in accordance with the method of Choi et al. (2005) using the glutamate dehydrogenase coupled assay. Briefly, a reaction mixture containing 4 mM $CaCl_2$, 10 mM α -ketoglutarate, 0.2 U/ml glutamate dehydrogenase, 0.12 mM NADH, 20 μg TG2, and 10 mM Cbz-Gln-Gly in 200 mM 3-(*N*-morpholino)ethanesulfonic acid (pH 7.1) was used in the assay. The enzyme reaction was initiated by the addition of TG2 and the consumption of NADH was monitored using different concentrations of inhibitor (10–500 nM) by UV spectroscopy (340 nm, $\epsilon = 6,220 \text{ cm}^{-1} \text{ M}^{-1}$). Kinetic parameters ($Kinact$ and Ki) were obtained using the Dynafit 4.05.129 software (Kuzmic, 1996, 2009).

Cell Permeability Assay

By Measuring Inactivation of Intracellular TG2

To induce intracellular TG2 activity, HUVECs with high endogenous TG2 were incubated with fresh growth medium with 0.5% FBS containing 1 μM ionomycin and 1 mM biotin-cadaverine (Zedira) in the presence or absence of 50 μM of TG2 inhibitors 3h, 1f, 3f, 3e, and 1e. The non-cell-permeable inhibitor R281 and the cell-permeable inhibitor R283 were used as the negative and positive controls, respectively. After a 3-hr incubation, the cells were collected in homogenization buffer (50 mM Tris-HCl [pH 7.5], 150 mM NaCl, 1 mM EDTA) and sonicated on ice. The cell membrane was pelleted at $60,000 \times g$ for 60 min and the supernatant (the cytosol fraction) was used for the assay. 50 μg of total protein in 100 μl of the homogenization buffer was used in the biotin-cadaverine incorporation assay as described previously by Wang et al. (2012).

By the In Vitro Passive Cellular Permeability Assay

The permeability (P exact) of 3h, 1h, 3e across an MDCK-MDR1 cell monolayer was measured at a starting concentration of 3 μM in the presence of GF120918, an efflux inhibitor. The pH of the donor and receiver compartments was 7.4 (Hank's balanced salt solution).

Incubations were carried out in an atmosphere of 5% CO_2 with a relative humidity of 95% at 37°C for 60 min. Apical and basolateral samples were diluted for analysis by liquid chromatography-tandem mass spectrometry. The integrity of the monolayers throughout the experiment was checked by monitoring Lucifer yellow permeation using fluorimetric analysis (Tran et al., 2004).

Western Blotting for the Dansyl Inhibitor Interaction with rhTG2

1 μg of recombinant human TG2 (rhTG2), wt or the active site C277S mutant protein, was incubated with the dansylated TG2 inhibitor 1h at 100 μM and 50 μM in the presence of 10 mM Ca^{2+} and 1 mM DTT in Tris-HCl buffer (pH 7.4) for 30 min at room temperature. The primary amine substrate MDC, which is incorporated into the available γ -glutamyl residues of TG2 by the enzyme, was used as the positive signal control sample, while non-labeled rhTG2 was used as the negative control. The reaction was stopped by diluting the samples into 2 \times Laemmli buffer and boiling at 95°C for 5 min. The presence of dansyl was detected via western blotting (Wang et al., 2012, 2013) by using a specific anti-dansyl antibody (Invitrogen).

The Targeting of In Situ TG2 Activity by Fluorescence Microscopy Using the Dansyl Inhibitor 3h

HUVECs and TG2 $^{-/-}$ mouse endothelial cells were used in this study. HUVECs were treated with 1 μM ionomycin in the presence or absence of 50 μM of 3e to pre-block the intracellular active TG2 for 3 hr, and the cells were further treated with 5 μM 3h for another 2 hr. TG2 $^{-/-}$ endothelial cells were treated in a comparable manner but were not exposed to the inhibitor 3e. For detection of endogenous TG2 activity, HUVECs were incubated without ionomycin. After the incubation, the cells were washed three times with pre-chilled methanol and fixed with methanol for 20 min at -20°C . Following blocking with 3% BSA in PBS (pH 7.4) for 30 min at 37°C, the cells were incubated with rabbit anti-dansyl antibody and revealed using a

secondary tetramethylrhodamineisothiocyanate-conjugated antibody for a 2-hr incubation at 37°C. The fluorescence signal was visualized using a Zeiss epifluorescent microscope using a 60x objective.

Detection of TG2 Activity Using Co-IP

Immunoprecipitation of the intracellular TG2-dansyl inhibitor complex was performed following the treatment of cells with **3h** with or without pre-treatment of 50 μM **3e** (as described above). Cytosol fractions of HUVECs or NIH3T3 cells transduced with TG2 were collected as described above. Anti-TG2 antibody was used to pull down the TG2 immuno-complex and SDS-PAGE and western blotting were then performed to detect the presence of the dansyl group of **3h**. TG2 knockout endothelial cells or non-TG2 transduced NIH3T3 cells, as well as a mouse IgG negative control antibody, were used as the negative controls.

Animal Study

Animal studies were undertaken with full ethical approval and all procedures carried out under license according to regulations laid down by Her Majesty's Government, United Kingdom (Animals Scientific Procedures Act, 1986) and undertaken in accordance with the 3Rs. Two groups of five animals were used. In the first group, C57BL/6 male mice (14 weeks old) were infused with AngII 1.1 mg/kg/day in 50% DMSO in PBS (pH 7.4) for 2 weeks without TG2 inhibitor via a subcutaneously implanted osmotic pump (Alzet 1002) as previously described (Murdoch et al., 2014). In the second group, compound **3h** was infused in a similar manner at 25 mg/kg/day together with AngII in 50% DMSO in PBS (pH 7.4) over 14 days. After 14 days, kidneys from the treated mice were frozen in OCT (CellPath) at an optimal temperature (−150°C) using isopentane; subsequently, 6-μm sections were prepared. Picrosirius red staining was performed to measure collagen staining as previously reported (Murdoch et al., 2014). The collagen content was quantified as the percentage area in a minimum of ten images per mouse using Image-Pro Plus version 5.0 (Media Cybernetics). The concentration (270 mM) of inhibitor used in the pump was approximated from computer simulations to give the steady state concentration in the mouse assuming an extensive distribution of the drug at 5 μM with a half-life of 1 hr.

Statistical Analysis

Data are expressed as the mean ± SD for at least three independent replicate experiments ($n \geq 3$) unless otherwise stated. Statistical tests were undertaken using InStat (GraphPad). Statistical analysis of the results was undertaken using one-way ANOVA using a post-test depending on the requirement.

SUPPLEMENTAL INFORMATION

Supplemental Information includes Supplemental Experimental Procedures, four figures, and two tables and can be found with this article online at <http://dx.doi.org/10.1016/j.chembiol.2015.08.013>.

AUTHOR CONTRIBUTION

M.G., Z.W., and D.R. designed the experiments. E.B. performed the compound synthesis and the modeling, with D.R. Z.W., A.C., T.T., C.M., M.B., and S.E.L. performed the biological experiments, and all authors analyzed the data. M.G., Z.W., E.B., and D.R. wrote the manuscript.

ACKNOWLEDGMENTS

The authors acknowledge EPSRC National Mass Spectrometry Centre, Swansea (UK) for recording the high resolution mass spectra. To GlaxoSmithKline, UK, for undertaking the in vitro DMPK assays. Prof Soichi Kojima's group (Riken, Japan) for kindly providing the TG2 knockout endothelial cells. To Dr Raj K. Singh Badhan (Aston University) for help in calculating the inhibitor concentration used in the in vivo experiments following pharmacokinetic simulations. Fruitful discussions with Dr Alexandre Mongeot and Dr Russell Collighan (Aston University) are also acknowledged. M.G. was the major grant holder that funded the work. E.B. was supported by a Marie Curie research grant ("TRANSCOM", FP7 No: 251506). A.C. was supported by a Marie Curie

research grant ("TRANSPATH", FP7 No 289964). None of the authors of this manuscript have a financial interest related to this work.

Received: April 9, 2015

Revised: August 4, 2015

Accepted: August 18, 2015

Published: October 8, 2015

REFERENCES

- Badarau, E., Collighan, R.J., and Griffin, M. (2013a). Recent advances in the development of tissue transglutaminase (TG2) inhibitors. *Amino Acids* 44, 119–127.
- Badarau, E., Mongeot, A., Collighan, R.J., Rathbone, D.L., and Griffin, M. (2013b). Imidazolium-based warheads strongly influence activity of water-soluble peptidic transglutaminase inhibitors. *Eur. J. Med. Chem.* 66, 526–530.
- Baumgartner, W., Golenhofen, N., Weth, A., Hiiragi, T., Saint, R., Griffin, M., and Drenckhahn, D. (2004). Role of transglutaminase 1 in stabilisation of intercellular junctions of the vascular endothelium. *Histochem. Cell Biol.* 122, 17–25.
- Bergamini, C.M., Collighan, R.J., Wang, Z., and Griffin, M. (2011). Structure and regulation of type 2 transglutaminase in relation to its physiological functions and pathological roles. *Adv. Enzymol. Relat. Areas Mol. Biol.* 78, 1–46.
- Colak, G., Keillor, J.W., and Johnson, G.V. (2011). Cytosolic guanine nucleotide binding deficient form of transglutaminase 2 (R580a) potentiates cell death in oxygen glucose deprivation. *PLoS One* 6, e16665.
- Choi, K., Siegel, M., Piper, J.L., Yuan, L., Cho, E., Strnad, P., Omary, B., Rich, K.M., and Khosla, C. (2005). Chemistry and biology of dihydroisoxazole derivatives: selective inhibitors of human transglutaminase 2. *Chem. Biol.* 12, 469–475.
- Duval, E., Case, A., Stein, R.L., and Cuny, G.D. (2005). Structure-activity relationship study of novel tissue transglutaminase inhibitors. *Bioorg. Med. Chem. Lett.* 15, 1885–1889.
- Freund, K.F., Doshi, K.P., Gaul, S.L., Claremon, D.A., Remy, D.C., Baldwin, J.J., Pitzberger, S.M., and Stern, A.M. (1994). Transglutaminase inhibition by 2-[(2-oxopropyl)thio]imidazolium derivatives: mechanism of factor XIIIa inactivation. *Biochemistry* 33, 10109–10119.
- Fukui, M., Kuramoto, K., Yamasaki, R., Shimizu, Y., Itoh, M., Kawamoto, T., and Hitomi, K. (2013). Identification of a highly reactive substrate peptide for transglutaminase 6 and its use in detecting transglutaminase activity in the skin epidermis. *FEBS J.* 280, 1420–1429.
- Griffin, M., Casadio, R., and Bergamini, C.M. (2002). Transglutaminases: nature's biological glues. *Biochem. J.* 368, 377–396.
- Griffin, M., Mongeot, A., Collighan, R., Saint, R.E., Jones, R.A., Coutts, I.G., and Rathbone, D.L. (2008). Synthesis of potent water-soluble tissue transglutaminase inhibitors. *Bioorg. Med. Chem. Lett.* 18, 5559–5562.
- Han, B.G., Cho, J.W., Cho, Y.D., Jeong, K.C., Kim, S.Y., and Lee, B.I. (2010). Crystal structure of human transglutaminase 2 in complex with adenosine triphosphate. *Int. J. Biol. Macromol.* 47, 190–195.
- Hand, D., Bungay, P.J., Elliott, B.M., and Griffin, M. (1985). Activation of transglutaminase at calcium levels consistent with a role for this enzyme as a calcium receptor protein. *Biosci. Rep.* 5, 1079–1086.
- Hitomi, K., Kitamura, M., and Sugimura, Y. (2009). Preferred substrate sequences for transglutaminase 2: screening using a phage-displayed peptide library. *Amino Acids* 36, 619–624.
- Huang, L., Haylor, J.L., Hau, Z., Jones, R.A., Vickers, M.E., Wagner, B., Griffin, M., Saint, R.E., Coutts, I.G., El Nahas, A.M., et al. (2009). Transglutaminase inhibition ameliorates experimental diabetic nephropathy. *Kidney Int.* 76, 383–394.
- Johnson, T.S., Fisher, M., Haylor, J.L., Hau, Z., Skill, N.J., Jones, R., Saint, R., Coutts, I., Vickers, M.E., El Nahas, A.M., et al. (2007). Transglutaminase inhibition reduces fibrosis and preserves function in experimental chronic kidney disease. *J. Am. Soc. Nephrol.* 18, 3078–3088.

- Klock, C., Jin, X., Choi, K., Khosla, C., Madrid, P.B., Spencer, A., Raimundo, B.C., Boardman, P., Lanza, G., and Griffin, J.H. (2011). Acylideneoxindoles: a new class of reversible inhibitors of human transglutaminase 2. *Bioorg. Med. Chem. Lett.* *21*, 2692–2696.
- Klock, C., Herrera, Z., Albertelli, M., and Khosla, C. (2014). Discovery of potent and specific dihydroisoxazole inhibitors of human transglutaminase 2. *J. Med. Chem.* *57*, 9042–9064.
- Kuzmic, P. (1996). Program DYNFIT for the analysis of enzyme kinetic data: application to HIV proteinase. *Anal. Biochem.* *237*, 260–273.
- Kuzmic, P. (2009). DynaFit—a software package for enzymology. *Methods Enzymol.* *467*, 247–280.
- Liu, S., Cerione, R.A., and Clardy, J. (2002). Structural basis for the guanine nucleotide-binding activity of tissue transglutaminase and its regulation of transamidation activity. *Proc. Natl. Acad. Sci. USA* *99*, 2743–2747.
- Lortat-Jacob, H., Burhan, I., Scarpellini, A., Thomas, A., Imberty, A., Vivès, R.R., Johnson, T., Gutierrez, A., and Verderio, E.A. (2012). Transglutaminase-2 interaction with heparin: identification of a heparin binding site that regulates cell adhesion to fibronectin-transglutaminase-2 matrix. *J. Biol. Chem.* *287*, 18005–18017.
- Murdoch, C.E., Chaubey, S., Zeng, L., Yu, B., Ivetic, A., Walker, S.J., Vanhoutte, D., Heymans, S., Grieve, D.J., Cave, A.C., et al. (2014). Endothelial NADPH oxidase-2 promotes interstitial cardiac fibrosis and diastolic dysfunction through proinflammatory effects and endothelial-mesenchymal transition. *J. Am. Coll. Cardiol.* *63*, 2734–2741.
- Ozaki, S., Ebisui, E., Hamada, K., Goto, J., Suzuki, A.Z., Terauchi, A., and Mikoshiba, K. (2010). Potent transglutaminase inhibitors, aryl beta-aminoethyl ketones. *Bioorg. Med. Chem. Lett.* *20*, 1141–1144.
- Ozaki, S., Ebisui, E., Hamada, K., Suzuki, A.Z., Terauchi, A., and Mikoshiba, K. (2011). Potent transglutaminase inhibitors, dithio beta-aminoethyl ketones. *Bioorg. Med. Chem. Lett.* *21*, 377–379.
- Pardin, C., Pelletier, J.N., Lubell, W.D., and Keillor, J.W. (2008a). Cinnamoyl inhibitors of tissue transglutaminase. *J. Org. Chem.* *73*, 5766–5775.
- Pardin, C., Roy, I., Lubell, W.D., and Keillor, J.W. (2008b). Reversible and competitive cinnamoyl triazole inhibitors of tissue transglutaminase. *Chem. Biol. Drug Des.* *72*, 189–196.
- Pavlyukov, M.S., Antipova, N.V., Balashova, M.V., and Shakhparonov, M.I. (2012). Detection of transglutaminase 2 conformational changes in living cell. *Biochem. Biophys. Res. Commun.* *421*, 773–779.
- Perez Alea, M., Kitamura, M., Martin, G., Thomas, V., Hitomi, K., and El Alaoui, S. (2009). Development of an isoenzyme-specific colorimetric assay for tissue transglutaminase 2 cross-linking activity. *Anal. Biochem.* *389*, 150–156.
- Pinkas, D.M., Strop, P., Brunger, A.T., and Khosla, C. (2007). Transglutaminase 2 undergoes a large conformational change upon activation. *PLoS Biol.* *5*, 2788–2795.
- Prime, M.E., Andersen, O.A., Barker, J.J., Brooks, M.A., Cheng, R.K., Toogood-Johnson, I., Courtney, S.M., Brookfield, F.A., Yarnold, C.J., Marston, R.W., et al. (2012). Discovery and structure-activity relationship of potent and selective covalent inhibitors of transglutaminase 2 for Huntington's disease. *J. Med. Chem.* *55*, 1021–1046.
- Scarpellini, A., Huang, L., Burhan, I., Schroeder, N., Funck, M., Johnson, T.S., and Verderio, E.A. (2014). Syndecan-4 knockout leads to reduced extracellular transglutaminase-2 and protects against tubulointerstitial fibrosis. *J. Am. Soc. Nephrol.* *25*, 1013–1027.
- Schaertl, S., Prime, M., Wityak, J., Dominguez, C., Munoz-Sanjuan, I., Pacifici, R.E., Courtney, S., Scheel, A., and Macdonald, D. (2010). A profiling platform for the characterization of transglutaminase 2 (TG2) inhibitors. *J. Biomol. Screen.* *15*, 478–487.
- Schoellmann, G., and Shaw, E. (1963). Direct evidence for the presence of histidine in the active center of chymotrypsin. *Biochemistry* *2*, 252–255.
- Tran, T.T., Mittal, A., Gales, T., Maleeff, B., Aldinger, T., Polli, J.W., Ayrton, A., Ellens, H., and Bentz, J. (2004). Exact kinetic analysis of passive transport across a polarized confluent MDCK cell monolayer modeled as a single barrier. *J. Pharm. Sci.* *93*, 2108–2123.
- Wang, Z., and Griffin, M. (2012). TG2, a novel extracellular protein with multiple functions. *Amino Acids* *42*, 939–949.
- Wang, Z., and Griffin, M. (2013). The role of TG2 in regulating S100A4-mediated mammary tumour cell migration. *PLoS One* *8*, e57017.
- Wang, Z., Collighan, R.J., Pytel, K., Rathbone, D.L., Li, X., and Griffin, M. (2012). Characterization of heparin-binding site of tissue transglutaminase: its importance in cell surface targeting, matrix deposition, and cell signaling. *J. Biol. Chem.* *287*, 13063–13083.
- Wang, Z., Perez, M., Caja, S., Melino, G., Johnson, T.S., Lindfors, K., and Griffin, M. (2013). A novel extracellular role for tissue transglutaminase in matrix-bound VEGF-mediated angiogenesis. *Cell Death Dis.* *4*, e808.
- Wityak, J., Prime, M.E., Brookfield, F.A., Courtney, S.M., Erfan, S., Johnsen, S., Johnson, P.D., Li, M., Marston, R.W., Reed, L., et al. (2012). SAR development of lysine-based irreversible inhibitors of transglutaminase 2 for Huntington's disease. *ACS Med. Chem. Lett.* *3*, 1024.
- Zhang, J., Antonyak, M.A., Singh, G., and Cerione, R.A. (2013). A mechanism for the upregulation of EGF receptor levels in glioblastomas. *Cell Rep.* *3*, 2008–2020.